IEEE Open Journal of
Industry Applications

Received 11 June 2021; revised 30 September 2021; accepted 11 October 2021. Date of publication 15 October 2021;
date of current version 1 November 2021. The review of this article was arranged by Associate Editor Petros Karamanakos.

Digital Object Identifier 10.1109/OJIA.2021.3120427

Reduced-Sensors-Based Predictive Controller for LC Filtered Four-Leg Inverters

D. XIAO (Member, IEEE), K. S. ALAM (Member, IEEE), R. DUTTA (Senior Member, IEEE), AND M. F. RAHMAN (Fellow, IEEE)

EET, UNSW, Sydney 2052, New South Wales, Australia

CORRESPONDING AUTHOR: DAN XIAO (e-mail: d.xiao@unsw.edu.au)

ABSTRACT The high number of sensors, ten in total, required by the traditional finite control set model predictive control (FCS-MPC) strategy of a four-leg inverter with LC output filter increases the complexity and cost of the system and limits the practical application and commercialization. To simplify the implementation, reduce the cost and enhance the reliability, a novel current sensorless predictive load voltage control scheme, with only four voltage sensors and no current sensors, is proposed in this work. A new dynamic model of the LC filtered four-leg inverter is constructed in the stationary ($\alpha\beta\gamma$) reference frame for the proposed load voltage and capacitor current observer. The dual-boundary-layer nonlinear feedback is combined with a linear feedback term to enhance the robustness while retaining the accuracy of the observer. Extensive experiments are performed to confirm the effectiveness of the proposed controller. The results validate that the proposed sensor-less FCS-MPC with only four voltage sensors achieves an equivalent performance to the conventional FCS-MPC with ten sensors.

INDEX TERMS LC filter, DC-AC power converter, distributed generation system, prediction.

I. INTRODUCTION

LC filtered four-leg inverter has been considered as a promising solution for providing sinusoidal output voltages in non-linear and unbalanced loading conditions [1]–[2]. Compared to a three-leg inverter, this power converter offers several benefits including higher utilization of DC-link voltage, reduced ripple in DC-link voltage, requirement of lower DC-bus capacitance, and ability to handle non-linear and unbalanced loads effectively [1]–[2]. In standalone applications LC filtered four-leg inverters are commonly used to control the load voltage [2]. To achieve a sinusoidal-shaped output load voltage, various control schemes have been investigated including sliding mode controllers [2], dead-beat controller [3], repetitive and resonant controllers [4], and predictive control [5].

FCS-MPC for power converters offers simplicity, the capability to handle multiple control objectives and fast dynamic response [6]–[7]. Moreover, the absence of a modulator in the FCS-MPC technique allows the exclusion of a complicated three-dimensional space vector modulation (3D-SVM), thereby offering simplicity in the digital implementation [7]. Nevertheless, to predict the load voltage, the FCS-MPC technique for 4-leg converters with an LC filter needs six current sensors for the inverter and load current measurements, three voltage sensors for the load voltage measurements and one voltage sensor for the DC-bus voltage measurement [7]. The high number of sensors (ten in total) increases the cost and volume of the inverter system [8]. In contrast, sensor-less control can reduce the cost and size of the system as well as the measurement power losses, thereby enhancing the reliability of system. Furthermore, it ensures the continuous operation of the system under faulty sensor conditions [8].

The above-mentioned advantages have led to extensive investigations related to sensor-less control to reduce the voltage and current sensors in different power converters [8]–[11]. Recently, sensor-less technique has been extended to FCS-MPC approach [12]–[14] to control the 3-leg power converters such as grid-connected converter with L-filters [15], LC filters [16] or LCL filters[17]. Application of sensor-less predictive control method has also been widely extended for motor drive applications [18]–[19]. For the grid voltage sensor-less predictive control approach, different types of observers can be utilized to estimate the grid voltage [12]. A sliding mode observer-based source voltage sensor-less predictive current control is proposed in [12] for 3-leg voltage

source converters with inductive filters. This combination results in the reduction in volume and cost of the system with increased reliability [12]–[14]. An alternate approach is to utilize a hybrid parallel observer for grid voltage sensor-less predictive current control implementation as presented in [14]. Elimination of load current sensors is achieved in [20] for a standalone 3-leg VSI with LC filter. However, inductor current sensors are not eliminated with this method.

The existing control methods with a reduced number of sensors [8]–[11] cannot be directly applied to the current sensor-less control of standalone 4-leg VSIs with LC-filter or combined with FCS-MPC. This is because the load current and inductor current cannot be simultaneously observed by the load voltage if the traditional dynamic model of the four-leg inverter is used. Therefore, the conventional dynamic model [8]–[11] cannot be directly used for current sensor-less observer design. Addressing this issue is the main novelty and contribution of this paper. To eliminate all the six current sensors in FCS-MPC for four-leg inverters with LC filter, a combined sliding mode observer is proposed for predictive load voltage control in this paper. Re-design of the traditional FCS-MPC is presented by removing the need for the inductor and load current measurement. The plant model has been re-arranged to be based on the capacitor current and load voltage and an estimator of the capacitor current has been introduced. The performances of the new controller and the traditional FCS-MPC are compared by experiments. Extensive experimental results verify that the proposed method retains the high performance of traditional FCS-MPC while the simplicity, reliability, and cost are enhanced compared to the conventional method. The novelty and contributions of the proposed control scheme are:

- A new current sensor-less technique for implementing FCS-MPC of an LC filtered four-leg inverter is proposed in this paper. Until now, no current sensor-less control technique is available for this topology. Until now, there is no research reported yet for the reduced sensor-based or current sensor-less FCS-MPC of the 4-leg VSIs with LC filter [7]. The proposed current sensor-less control scheme is the first presentation for 4-leg LC-filtered VSIs with no current sensors required.
- The existing current observers cannot be directly combined with the FCS-MPC to realize the current sensor-less control of VSIs with LC-filter. To solve this issue, a new dynamic model of the four-leg inverter is developed in this paper considering the capacitor current and load voltage as the state variables. Based on this modified dynamic model, a load voltage and filter capacitor current observer is introduced to eliminate all six current transducers required by the FCS-MPC approach for a LC filtered four-leg inverter.

II. PREDICTION MODEL OF A 4-LEG VSI WITH LC FILTER

FCS-MPC approach reported in [7] utilizes the state equations in *abc* reference frame which suffers from strong coupling among the phases due to the neutral leg inductor. The model of four-leg inverter with an LC filter (referred to the block

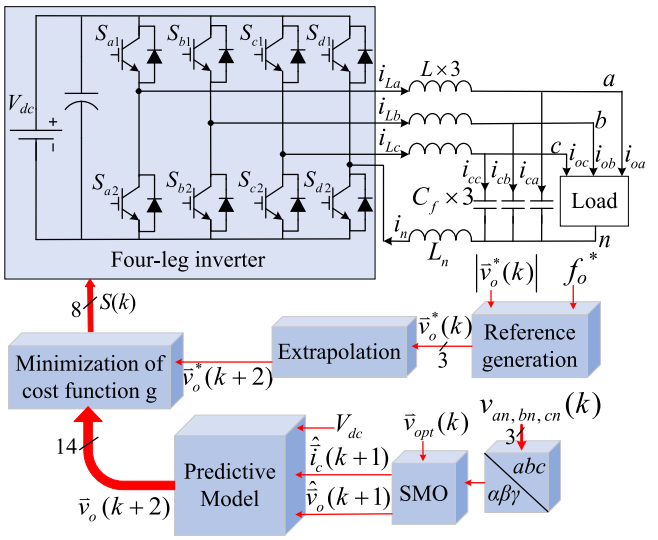

FIGURE 1. Simplified block diagram of the current sensor-less method proposed in this work.

diagram of the proposed method shown in Fig. 1) is described in $\alpha\beta\gamma$ reference frame [3], eliminating the coupling impact in *abc* reference frame as:

$$\frac{d}{dt}\begin{bmatrix} i_{L\alpha} \\ i_{L\beta} \\ i_{L\gamma} \end{bmatrix} = \begin{bmatrix} 1/L & 0 & 0 \\ 0 & 1/L & 0 \\ 0 & 0 & 1/(L+3L_n) \end{bmatrix} \begin{bmatrix} v_{\alpha f} - v_{\alpha n} \\ v_{\beta f} - v_{\beta n} \\ v_{\gamma f} - v_{\gamma n} \end{bmatrix} \tag{1}$$

where L is, L_n are the filter inductance, neutral leg inductance, C_f is the filter capacitance. The $\alpha\beta\gamma$ components of the load voltages are represented as $v_{\alpha n}$, $v_{\beta n}$ and $v_{\gamma n}$, while the $\alpha\beta\gamma$ components of the filter inductor current are $i_{L\alpha}$, $i_{L\beta}$ and $i_{L\gamma}$. $v_{\alpha f}$, $v_{\beta f}$ and $v_{\gamma f}$ are the $\alpha\beta\gamma$ components of the converter voltages. $\alpha\beta\gamma$ components of the load current are expressed as $i_{o\alpha}$, $i_{o\beta}$ and $i_{o\gamma}$.

$$\frac{d}{dt}\begin{bmatrix} v_{\alpha n} \\ v_{\beta n} \\ v_{\gamma n} \end{bmatrix} = \frac{1}{C_f}\begin{bmatrix} i_{L\alpha} - i_{o\alpha} \\ i_{L\beta} - i_{o\beta} \\ i_{L\gamma} - i_{o\gamma} \end{bmatrix} \tag{2}$$

Considering the high sampling frequency ($f_s/f \gg 20$), the derivatives can be approximated as highlighted in [3]. It should be noted that this approximation is widely used in the existing literature for inverters equipped with LC filter [3]. Thus, the α component of the inductor current and load voltage vectors are written in discrete form as [2]–[3]:

$$i_{L\alpha}[k+1] = i_{L\alpha}[k] + \frac{T_s}{L}(v_{\alpha f}[k] - v_{\alpha n}[k]) \tag{3}$$

$$v_{\alpha n}[k+1] = \frac{T_s}{C_f}(i_{L\alpha}[k] - i_{o\alpha}[k]) + v_{\alpha n}[k] \tag{4}$$

where T_s is the sampling interval.

Similar equations can be obtained for β and γ components. A discrete model of the VSI is used to predict the output load voltage (as in (3)-(4)). As suggested in [7], a simple delay compensation approach is employed to compensate the delay

in control implementation. The MPC cost function is chosen as:

$$g = \sum_{x=\alpha,\beta,\gamma} (v_{xn}^* - v_{xn}[k+2])^2 \tag{5}$$

where $\alpha\beta\gamma$ components of the output load voltage reference values are represented by $v_{\alpha n}^*$, $v_{\beta n}^*$ and $v_{\gamma n}^*$. The optimization problem is formulated as:

$$\vec{U}_{opt}[k] = \arg\{\min_{\vec{U}_i[k]} g\}, \quad i = 0..15 \tag{6}$$

where $\vec{U}_i[k] = [u_{\alpha f}, u_{\beta f}, u_{\gamma f}]_i^T$ refers to 16 voltage vectors of the inverter and $\vec{U}_{opt}[k]$ is the optimal voltage vector of the inverter. As can be seen from (3)-(4), the prediction of load voltage requires the measurement of load currents, filter inductor currents, and load voltages. Due to the unbalanced nature of the loads, as many as ten sensors are used in FCS-MPC controlled four-leg inverter, which imposes a major limitation for the practical implementation and commercialization.

III. PROPOSED METHOD

A. RECONSTRUCTION OF THE DYNAMIC MODEL OF FOUR-LEG INVERTER

The existing dynamic model of the four-leg inverter is expressed as (for simplicity only α component is shown in this Section):

$$\frac{d}{dt}X = AX + Bu$$
$$Y = CX \tag{7}$$

where

$$C = \begin{bmatrix} 1 & 0 & 0 \\ 0 & 1 & 0 \end{bmatrix}, \; B = \begin{bmatrix} 1/L \\ 0 \\ 0 \end{bmatrix},$$
$$A = \begin{bmatrix} 0 & -1/L & 0 \\ 1/C_f & 0 & -1/C_f \\ 0 & 0 & 0 \end{bmatrix},$$
$$X = \begin{bmatrix} i_{L\alpha} & v_{\alpha n} & i_{o\alpha} \end{bmatrix}^T, u = v_{\alpha f} \tag{8}$$

If all the current sensors are eliminated, the output matrix Y has to only contain the elements related to the load voltage. Therefore, the output matrix in the conventional dynamic model should be modified as:

$$C = \begin{bmatrix} 0 & 1 & 0 \end{bmatrix} \tag{9}$$

The observability matrix can be expressed as:

$$R = \begin{bmatrix} C & CA & CA^2 \end{bmatrix}^T \tag{10}$$

This can be computed as:

$$R = \begin{bmatrix} 0 & 1 & 0 \\ 1/C_f & 0 & -1/C_f \\ 0 & -1/LC_f & 0 \end{bmatrix} \tag{11}$$

The rank of the observability matrix is 2 which is less than 3, the number of state variables. This is because the first and third rows of matrix R are linearly dependent. The system is not completely observable, i.e., the load current and inductor current cannot be simultaneously observed by the load voltage. Hence, the existing dynamic model of the inverter cannot be directly used for the current sensor-less observer design. To facilitate the current sensor-less technique, it is necessary to develop a new dynamic model of the inverter. The dynamics of the filter current are expressed as (α component):

$$L\frac{di_{L\alpha}}{dt} = (v_{\alpha f} - v_{\alpha n}) \tag{12}$$

The load voltage (α component) can be expressed as:

$$\frac{dv_{\alpha n}}{dt} = \frac{1}{C_f} i_{c\alpha} \tag{13}$$

Filter current ($i_{L\alpha}$) is written as:

$$i_{L\alpha} = i_{c\alpha} + i_{o\alpha} \tag{14}$$

Differentiating both sides of (14) yields:

$$\frac{di_{L\alpha}}{dt} = \frac{di_{c\alpha}}{dt} + \frac{di_{o\alpha}}{dt} \tag{15}$$

The load current can be assumed constant during two adjacent sampling interval (i.e. $di_{o\alpha}/dt = 0$) considering the sampling period is much smaller than the fundamental period. This assumption has been widely used in the literature [21]–[22] for LC filtered voltage source inverters. As demonstrated in [21]–[23], the performance degradation caused by this assumption is negligible. This is because the sampling period is very small, the load current changes slowly and can be considered to be constant during each sampling cycle [23]. Thus, (15) can be approximated as:

$$\frac{di_{L\alpha}}{dt} = \frac{di_{c\alpha}}{dt} \tag{16}$$

Substituting (12) into (16) yields:

$$\frac{di_{c\alpha}}{dt} = \frac{di_{L\alpha}}{dt} = \frac{1}{L}(v_{\alpha f} - v_{\alpha n}) \tag{17}$$

Eqs. (13) and (17) can be discretized as:

$$i_{c\alpha}[k+1] = i_{c\alpha}[k] + \frac{T_s}{L}(v_{\alpha f}[k] - v_{\alpha n}[k])$$
$$v_{\alpha n}[k+1] = v_{\alpha n}[k] + \frac{T_s}{C_f} i_{c\alpha}[k] \tag{18}$$

Similarly, for β and γ components, following equations are obtained:

$$i_{c\beta}[k+1] = i_{c\beta}[k] + \frac{T_s}{L}(v_{\beta f}[k+1] - v_{\beta n}[k])$$
$$v_{\beta n}[k+1] = v_{\beta n}[k] + \frac{T_s}{C_f} i_{c\beta}[k] \tag{19}$$

$$i_{c\gamma}[k+1] = i_{c\gamma}[k] + \frac{T_s}{L+3L_n}(v_{\gamma f}[k+1] - v_{\gamma n}[k])$$
$$v_{\gamma n}[k+1] = v_{\gamma n}[k] + \frac{T_s}{C_f} i_{c\gamma}[k] \tag{20}$$

Eqs. (18)-(20) describe a new dynamic model of the inverter which is used for current sensor-less control. As can be seen from this new dynamic model that the capacitor currents are observable from the load voltage and inverter voltage without any current information. This is because the number of state variables, filter capacitor current and the load voltage, is reduced to two for each phase. This number is the same as the rank of the observability matrix as in (11). This allows the elimination of all six current sensors.

B. COMBINED SLIDING MODE OBSERVER FOR CAPACITOR CURRENT ESTIMATION

By using the modified model of the 4-leg inverter, (18)-(20), a current observer can be derived and applied to the predictive control of LC filtered four-leg VSI. A combined sliding mode observer (SMO) is introduced. Based on the dynamic model of the VSI described by Eqs. (18)-(20), considering inverter voltage as the input, and load voltage and capacitor current as state variables, a combined sliding mode capacitor current observer can be formulated as:

$$\begin{bmatrix} \hat{v}_{\alpha n}[k+1] \\ \hat{i}_{c\alpha}[k+1] \end{bmatrix} = G \begin{bmatrix} \hat{v}_{\alpha n}[k] \\ \hat{i}_{c\alpha}[k] \end{bmatrix} + Bv_{\alpha f} + K \cdot e + H \cdot sgn_m(e) \quad (21)$$

where

$$K = \begin{bmatrix} k_1 T_s & 0 \\ k_2 T_s & 0 \end{bmatrix},\ X[k] = \begin{bmatrix} v_{\alpha n}[k] & i_{c\alpha}[k] \end{bmatrix}^T$$

$$\hat{X}[k] = \begin{bmatrix} \hat{v}_{\alpha n}[k] & \hat{i}_{c\alpha}[k] \end{bmatrix}^T,\ e = (X[k] - \hat{X}[k])$$

$$H = \begin{bmatrix} h_1 & 0 \\ h_2 & 0 \end{bmatrix},\ G = \begin{bmatrix} 1 & T_s/C_f \\ -T_s/L & 1 \end{bmatrix},\ B = \begin{bmatrix} 0 \\ T_s/L \end{bmatrix} \quad (22)$$

where $\hat{}$ denotes the estimated variables and K and H represent the feedback gain matrices. sgn_m function represents an improved sliding-mode component with dual-boundary-layer defined as [24]:

$$F = sgn_m(e) = \begin{cases} 1, & \text{if } e > b_2 \\ (e - b_1)/e_{max}, & \text{if } b_1 \le |e| \le b_2 \\ 0, & \text{if } |e| < b_1 \\ -1, & \text{if } e < -b_2 \end{cases} \quad (23)$$

where e is the estimation error, e_{max} is the maximum estimation error, $b_2 = b_1 + 1/(e/e_{max})$ and b_1 refers to the inner boundary layer width. A smaller value of b_1 can reduce the estimation error, e. However, chattering will be increased. Thus, b_1 is chosen to obtain a satisfactory estimation error with a minimal chattering. Within b_1 there is no non-linear activity in the observer as $F = 0$. When the estimation error increases due to parameter variation b_2 decreases and the non-linear feedback activity increases. This forces the estimation error to remain within an acceptable limit. The integration of non-linear term, sgn_m function in the observer improves the robustness of the observer toward parameter variation. The modified sgn_m function is illustrated in Fig. 2.

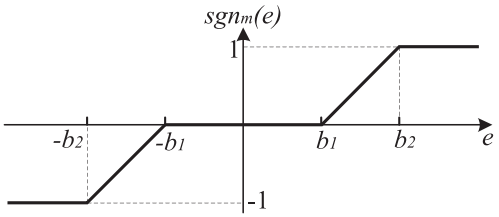

FIGURE 2. Illustration of improved sgn_m function.

C. DELAY COMPENSATION AND LOAD VOLTAGE PREDICTION

The predictive capability of the proposed observer allows a direct compensation for the one-step delay. The proposed observer estimates the values of load voltage and capacitor current at the $(k+1)^{th}$ sampling period as can be seen in (21). The one-step delay due to the digital implementation only needs to be compensated for the conventional method in this paper. Load voltages at $(k+1)^{th}$ sampling instant are computed by the observer as in (21) for the proposed method while computed by the prediction model as in (18) for the conventional method.

$$\hat{v}_{xn}[k+1] = v_{xn}[k] + \frac{T_s}{C_f}\hat{i}_{cx}[k] \quad (24)$$

where $x = \alpha, \beta, \gamma$.

Load voltages at $(k+2)$ sampling intervals is expressed as:

$$\hat{v}_{xn}[k+2] = \hat{v}_{xn}[k+1] + \frac{T_s}{C_f}\hat{i}_{cx}[k+1] \quad (25)$$

where $x = \alpha, \beta, \gamma$. The load voltage components are predicted with every fixed vector of the inverter by using (25) and used for cost function evaluation and minimization. It determines the optimal voltage vector of the inverter to be applied for the next sampling interval.

D. STABILITY ANALYSIS AND GAIN SELECTION AND OF THE OBSERVER

The gain matrix $\boldsymbol{K}$ can be selected from the pole assignment strategy with dead-beat property [20]. Subtracting the observer state equation (21) from the system dynamics yields the estimation error dynamics:

$$\tilde{X}[k+1] = (G - K)\tilde{X}[k] - H \cdot sgn_m(\tilde{X}[k]) \quad (26)$$

where $\tilde{X} = X - \hat{X}$.

The dynamics of error are dictated by the observer matrix $(G - K)$ eigenvalues. The stability of the proposed discrete observer is therefore asymptotically stable when $(G - K)$ has all the eigenvalues within the z-plane unit circle. The characteristic polynomial of the observer dynamic matrix is written as follows:

$$det(z\boldsymbol{I} - \boldsymbol{G} + \boldsymbol{K}) = z^2 + (k_1 T_s - 2)z + (1 - k_1 T_s) + \frac{T_s^2}{C_f}\left(k_2 + \frac{1}{L}\right) \quad (27)$$

TABLE 1 Parameters of the LC Filtered 4-Leg Inverter System

Variable	Description	Unit	Value
V_{dc}	DC-Bus voltage	V	240.0
L	Output filter inductance	mH	1.0
f	Base frequency	Hz	50.0
f_s	Sampling frequency	kHz	20.0
L_n	Neutral-point inductance	mH	1
C_f	Output filter capacitance	μF	84.0
v_o^*	Output voltage magnitude	V	0-100.0
b_1	Inner layer width of non-linear term	-	0.1
e_{max}	maximum estimation error	V	2.0

Zero eigenvalues correspond to the fastest transient performance of the estimator. To place both eigenvalues to a zero value the following relationship can be used. This will obtain the dead-beat property [23].

$$z^2 + (k_1 T_s - 2)z + (1 - k_1 T_s) + \frac{T_s^2}{C_f}\left(k_2 + \frac{1}{L}\right) = z^2 \quad (28)$$

By comparing the coefficients on both sides of (28), the observer gains $k1$ and $k2$ can be determined as

$$k_1 = \frac{2}{T_s}$$
$$k_2 = \frac{C_f}{T_s^2} - \frac{1}{L} \quad (29)$$

It should be noted that the estimator gain value (k_2) for γ component is different due to the involvement of additional neutral leg inductor and is obtained as:

$$k_2 = \frac{C_f}{T_s^2} - \frac{1}{L + 3L_n} \quad (30)$$

IV. EXPERIMENTAL RESULTS

Comparative experimental studies with the conventional FCS-MPC with ten sensors are carried out to validate the effectiveness of the proposed current sensor-less method as shown in Table-1).

Compared to the sensor-based MPC, the proposed scheme does not significantly increase the computational burden. The elimination of 6 current sensors allows the reduction of the A/D sample and conversion time and execution times for calibration and digital filtering for the current measurement compared to the conventional method. To validate that the proposed controller does not increase the computational cost, the computation times of both techniques are evaluated and compared. Execution times for sampling, A/D conversion, calibration, and filtering for multiplexed ADC channels are calculated for both methods in this comparison, as a high number of analog input channels are normally scanned by ADC module in the sequential mode in most of the cost-effective 32-bit micro-controllers. The execution time of the conventional sensor-based FS-MPC is 9.4 μs, including 6.36 μs for A/D conversion and 3.04 μs for the predictive control algorithm. Similarly, the execution time of the proposed controller

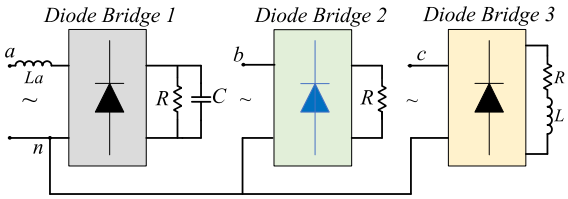

FIGURE 3. Single-phase nonlinear load circuit.

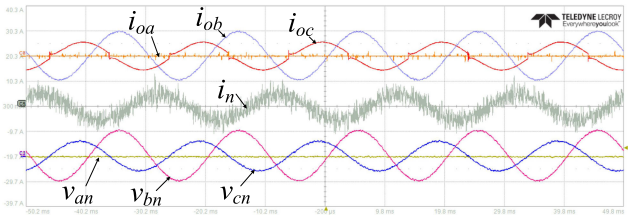

FIGURE 4. Case-A with 10-sensor based FCS-MPC method (output voltages: 100.0 Volts/Div, load currents: 5.0 A/Div, neutral inductor current: 10.0 A/Div and time: 20.0 ms/Div).

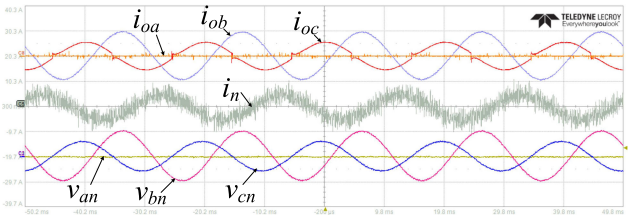

FIGURE 5. Case-A with the proposed method (output voltages: 100.0 Volts/Div, load currents: 5.0 A/Div, neutral inductor current: 10.0 A/Div and time: 20.0 ms/Div).

on the same control platform is 6.42 μs including 3.48 μs for the A/D conversion. This is because the current sensors are eliminated and thus 60% of the A/D conversion time for the current measurement is saved.

The following two case studies are performed to assess the performance of the proposed controller in steady-state:

- Case-A (voltage references are not balanced with non-linear loads as depicted in Fig. 3): $v_{an}^* = 50$ V, $v_{bn}^* = 100$ and $v_{cn}^* = 0$ V. $L_a = 4.7$ mH, $R_a = 20\ \Omega$, $C_a = 20\ \mu$F; $R_b = 20\ \Omega$; $R_c = 20\ \Omega$ and $L_c = 10$ mH.
- Case-B (voltage references are balanced and load are non-linear): $v_{an}^* = 100$ V, $v_{bn}^* = 100$ V and $v_{cn}^* = 100$ V; $L_a = 4.7$ mH, $R_a = 20\ \Omega$, $C_a = 20\ \mu$F; $R_b = 20\ \Omega$; $R_c = 20\ \Omega$ and $L_c = 10$ mH.

Case-A experimental results for the ten-sensor-based traditional method and the proposed method are shown in Figs. 4 and 5. The voltage reference for Phase c is set to zero while reference values for Phases a and b are 50 V and 100 V respectively. The output voltages v_{an} and v_{bn} track the their references irrespective of short-circuit in Phase-c ($v_{cn} = 0$) and nonlinear load connected to the output. The proposed method with only 4 voltage sensors achieves satisfactory performance in steady-state comparable to the conventional method with 10 sensors. Output load voltages FFT for the conventional

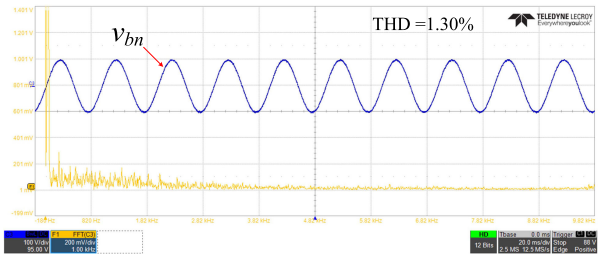

FIGURE 6. Output voltage (100.0 Volts/Div) and its harmonics spectrum (0.2 Volts/Div, 1.0 kHz/Div) in Case-A with 10-sensor based FCS-MPC method.

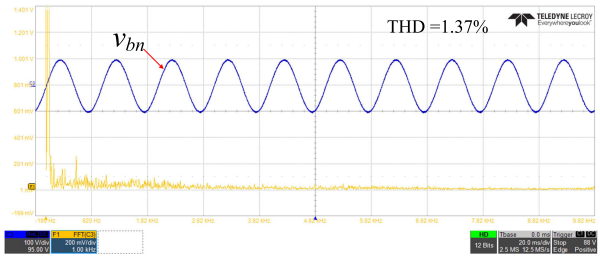

FIGURE 7. Output voltage (100.0 Volts/Div) and its harmonics spectrum (0.2 Volts/Div, 1.0 kHz/Div) in Case-A with the proposed sensorless method.

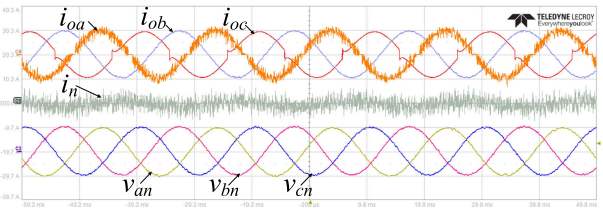

FIGURE 8. Case-B with 10-sensor based FCS-MPC method (output voltages: 100.0 Volts/Div, load currents: 5.0 A/Div, neutral inductor current: 10.0 A/Div and time: 20.0 ms/Div).

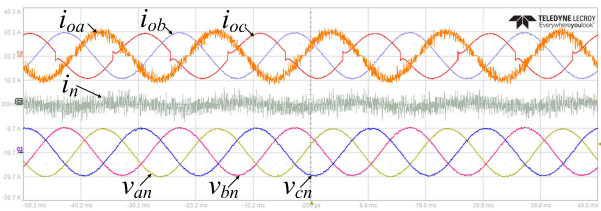

FIGURE 9. Case-B with the proposed method (output voltages: 100.0 Volts/Div, load currents: 5.0 A/Div, neutral inductor current: 10.0 A/Div and time: 20.0 ms/Div).

FCS-MPC and the proposed method are illustrated in Figs. 6 and 7 respectively. It can be seen that the proposed current sensor-less method obtains a similar steady-state performance compared to the conventional FCS-MPC that requires ten sensors, the THD of load voltage for Phase-a slightly increased from 1.30% to 1.37%.

The experimental results of ten-sensor-based FCS-MPC and proposed current sensorless methods in Case B are presented in Figs. 8 and 9. The load currents in Phase a and

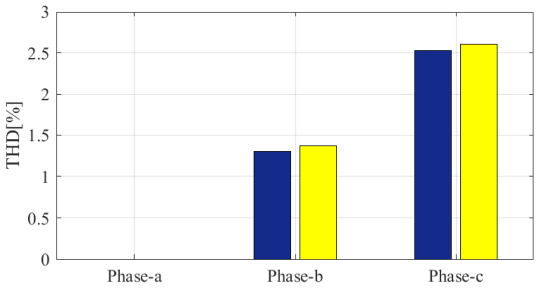

FIGURE 10. Load voltage THD comparison between the proposed method and 10-sensor based MPC in Case-A.

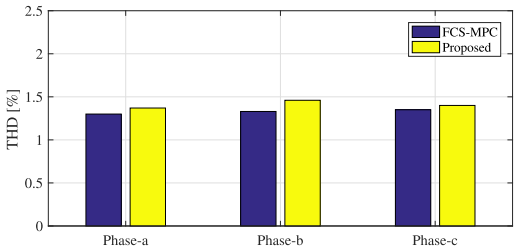

FIGURE 11. Load voltage THD compassion between 10-sensor based FCS-MPC and proposed method for Case-B.

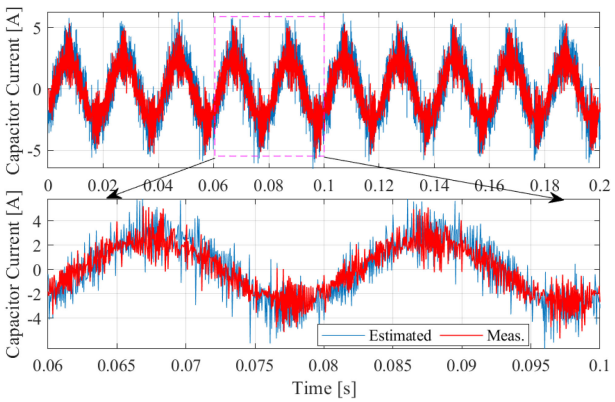

FIGURE 12. Experimental evaluation of the capacitor current estimation in Case B with the proposed method.

Phase c) are distorted due to the nonlinear load. However, the proposed scheme obtains a comparable performance to the 10-sensor-based method. The increment in the load voltage THD is within the acceptable range (less than 10% in the worst case) as illustrated in Figs. 10 and 11. The performance of the proposed current sensorless method relies on the estimation of the filter capacitor current and load voltage. Figs. 12 and 13 show the performance evaluation of the load voltage and capacitor current estimation in the proposed control method. It can be seen from Fig. 12 that the estimated capacitor current follows the actual capacitor current. As shown in Fig. 13, the load voltage track the sinusoidal reference very well even with a nonlinear load. The estimation error between the measured and estimated load voltages is very small in the proposed method. The proposed combined sliding mode observer

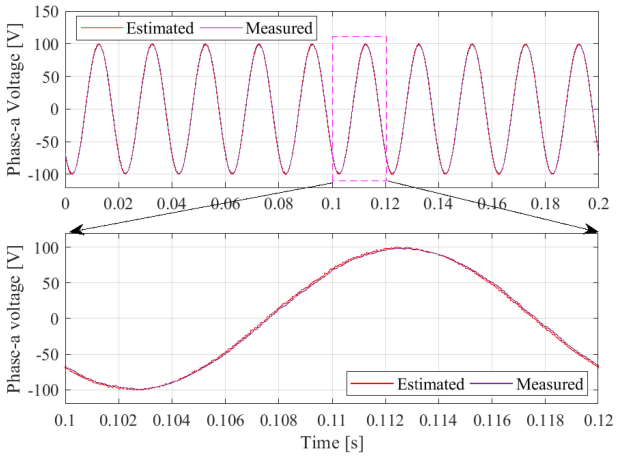

FIGURE 13. Experimental evaluation of the load voltage estimation in Case B with the proposed method.

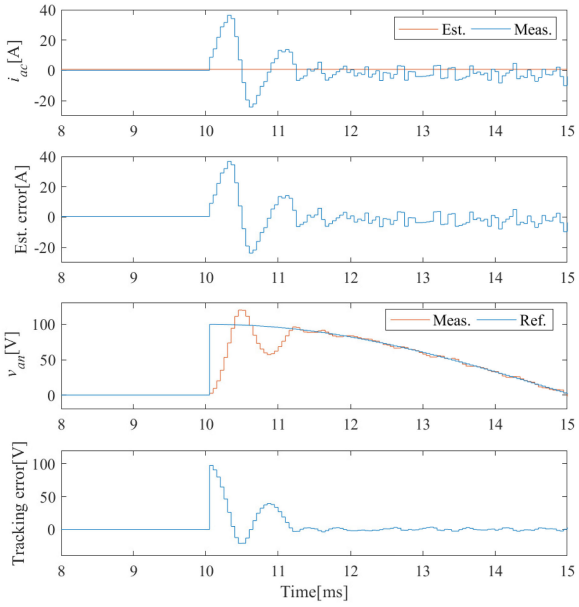

FIGURE 14. Transient performance of the conventional method (0 to 100 V).

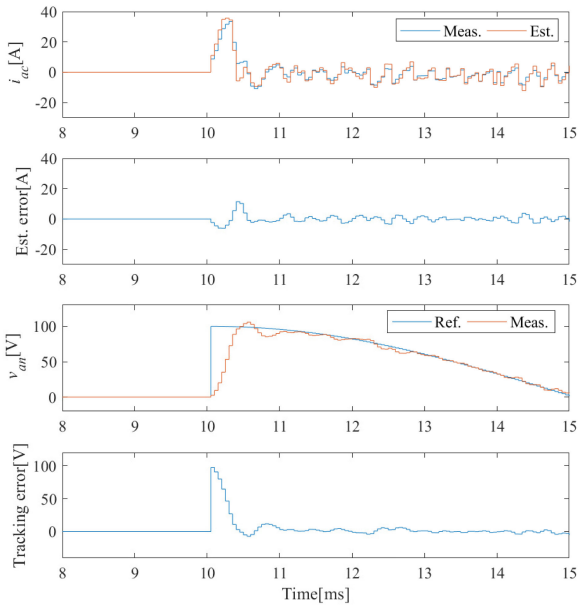

FIGURE 15. Transient performance of the proposed method (0 to 100 V).

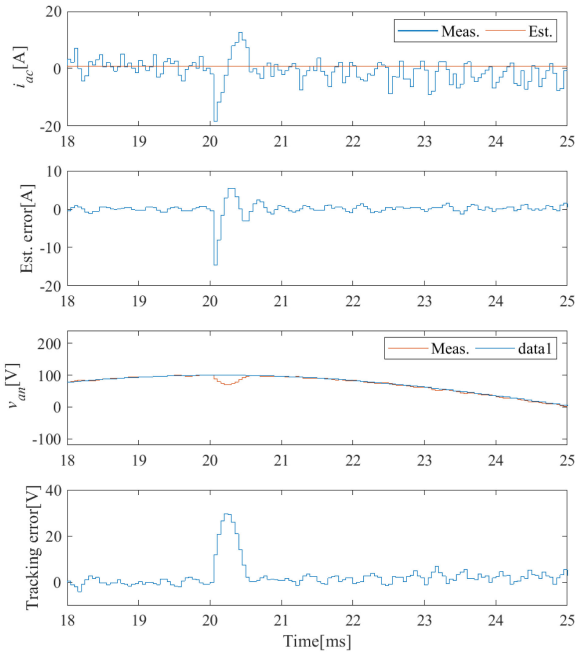

FIGURE 16. Transient performance of the conventional method (no load to full load).

provides a fairly consistent capacitor current and load voltage estimation matching their measured values. Observer gains and double boundary layers are carefully selected to ensure a reduced chattering and minimal estimation errors with satisfactory closed-loop dynamic performance.

To validate the efficacy of the proposed method, studies on transient performance are performed and compared with the conventional FCS-MPC. Figs. 14 and 15 show the experimental results for the load voltage transient response. It can be seen that the proposed sensor-less method achieves a similar dynamic response as the traditional FCS-MPC method. The load voltage overshoot is 20.9% for the conventional controller while 5.9% for the proposed controller. The estimated current converges to the actual capacitor current within 0.55 ms. The load disturbance test is performed by suddenly applying a large load from the no-load condition. This produces a large di_o/dt as the load is changed at the peak value of load voltage. As can be seen from Figs. 16 and 17, even with such a large load transient, the proposed controller is not affected and performs effectively. Both of the conventional and proposed controllers take 0.55 ms to drive the error to zero and maintain load voltage at the desired value irrespective of the large disturbance in the load. The current estimator also shows load adaptability and the convergence time, 0.75 ms,

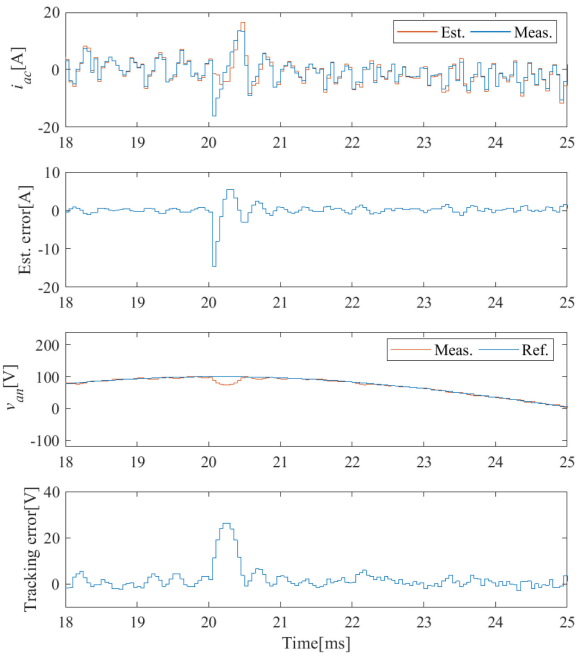

FIGURE 17. Transient performance of the proposed method (no load to full load).

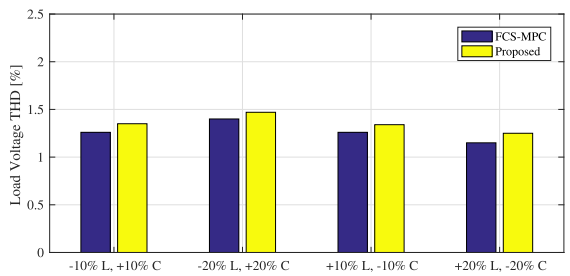

FIGURE 18. Load voltage THD comparison with variation of filter parameters.

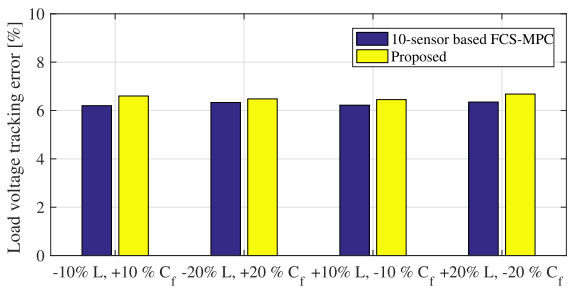

FIGURE 19. Comparison of steady-state error with the variation in filter parameters.

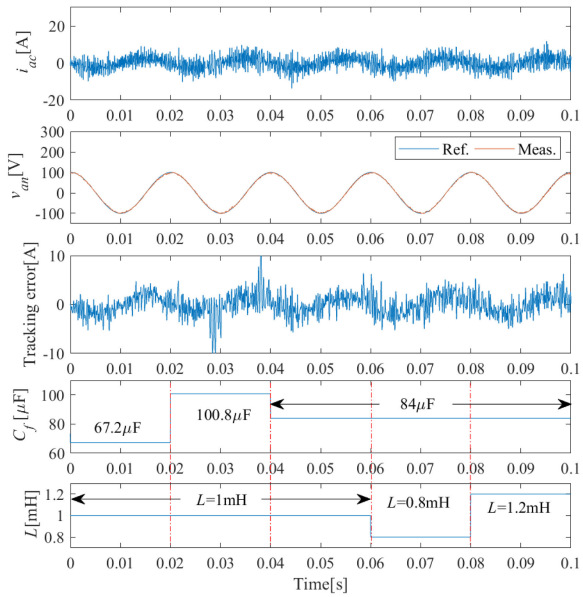

FIGURE 20. Robustness of the conventional method with ±20% filter parameter variations.

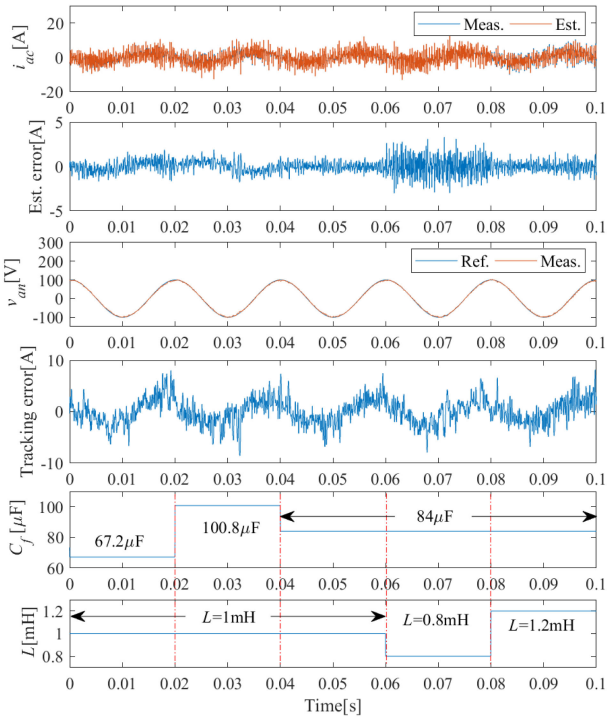

FIGURE 21. Robustness of the proposed method with ±20% filter parameter variations.

is less than 1/20th of the fundamental cycle with acceptable estimation error.

Furthermore, the steady-state tracking error and THD of the load voltage in the proposed method are compared to the conventional FCS-MPC with 10 sensors. The results shown in Figs. 18 and 19 validate that satisfactory robustness of the proposed method against variations in filter parameters. The robustness of the proposed methods against the variations of the output filter parameters during transient. The performance of the proposed controller is comparable to that of the conventional method as seen in Figs. 20 and 21. The instantaneous capacitor current, load voltage, tracking error, and estimation error are captured with nominal, underestimated, and overestimated values of the LC filter, respectively. It can be seen

that the estimated error in capacitor current is not affected when the capacitance is changed between 80% and 120% of nominal value. The average estimation error is zero and the tracking error of load voltage is not affected though higher estimation error spikes are observed when the inductance is reduced to 80% of nominal value. With 120% of nominal capacitance, there are sudden changes in the load voltage error near 0.03 s and 0.04 s. This also occurs in the load voltage of the conventional method. In conclusion, the robustness of the conventional sensor-based MPC method is retained in the proposed method.

V. CONCLUSION

A large quantity of voltage and current transducers (normally ten in total) is one of the main limitations of the predictive controller for an LC filtered four-leg inverter. To overcome this drawback, a combined sliding mode observer-based current sensor-less load voltage predictive control of four-leg inverters is proposed in this paper. The proposed method only requires four voltage sensors and eliminates all six current sensors. The dynamic model of the LC filtered four-leg VSI on the stationary ($\alpha\beta\gamma$) reference frame is re-arranged to make the capacitor current observable using load voltage and allow the elimination of six current sensors. Experimental results have been carried out in different operating conditions and verified the accuracy of the proposed controller. By using the proposed method, the overall size and cost of the FCS-MPC implementation for four-leg inverters is significantly reduced while the equivalent performance is retained compared to 10-sensors-based traditional FCS-MPC.

REFERENCES

[1] X. Guo, R. He, J. Jian, Z. Lu, X. Sun, and J. M. Guerrero, "Leakage current elimination of four-leg inverter for transformerless three-phase PV systems," *IEEE Trans. Power Electron.*, vol. 31, no. 3, pp. 1841–1846, Mar. 2016.

[2] M. Pichan and H. Rastegar, "Sliding-mode control of four-leg inverter with fixed switching frequency for uninterruptible power supply applications," *IEEE Trans. Ind. Electron.*, vol. 64, no. 8, pp. 6805–6814, Aug. 2017.

[3] M. Pichan, H. Rastegar, and M. Monfared, "Deadbeat control of the stand-alone four-leg inverter considering the effect of the neutral line inductor," *IEEE Trans. Ind. Electron.*, vol. 64, no. 4, pp. 2592–2601, Apr. 2017.

[4] A. Lidozzi, M. D. Benedetto, S. Bifaretti, L. Solero, and F. Crescimbini, "Resonant controllers with three degrees of freedom for AC power electronic converters," *IEEE Trans. Ind. Appl.*, vol. 51, no. 6, pp. 4595–4604, Nov./Dec. 2015.

[5] V. Yaramasu, M. Rivera, B. Wu, and J. Rodriguez, "Predictive control of four-leg power converters," in *Proc. IEEE Int. Symp. Predictive Control Elect. Drives Power Electron.*, 2015, pp. 121–125.

[6] M. Rivera, V. Yaramasu, A. Llor, J. Rodriguez, B. Wu, and M. Fadel, "Digital predictive current control of a three-phase four-leg inverter," *IEEE Trans. Ind. Electron.*, vol. 60, no. 11, pp. 4903–4912, Nov. 2013.

[7] V. Yaramasu, M. Rivera, M. Narimani, B. Wu, and J. Rodriguez, "Model predictive approach for a simple and effective load voltage control of four-leg inverter with an output *LC* filter," *IEEE Trans. Ind. Electron.*, vol. 61, no. 10, pp. 5259–5270, Oct. 2014.

[8] M. Mehreganfar, M. H. Saeedinia, S. A. Davari, C. Garcia, and J. Rodriguez, "Sensor-less predictive control of AFE rectifier with robust adaptive inductance estimation," *IEEE Trans. Ind. Informat.*, vol. 15, no. 6, pp. 3420–3431, Jun. 2019.

[9] J. Kukkola and M. Hinkkanen, "State observer for grid-voltage sensorless control of a converter equipped with an LCL filter: Direct discrete-time design," *IEEE Trans. Ind. Appl.*, vol. 52, no. 4, pp. 3133–3145, Jul./Aug. 2016.

[10] M. B. Ketzer and C. B. Jacobina, "Virtual flux sensor-less control for shunt active power filters with Quasi-resonant compensators," *IEEE Trans. Power Electron.*, vol. 31, no. 7, pp. 4818–4830, Jul. 2016.

[11] M. B. Ketzer and C. B. Jacobina, "Sensor-less control technique for PWM rectifiers with voltage disturbance rejection and adaptive power factor," *IEEE Trans. Ind. Electron.*, vol. 62, no. 2, pp. 1140–1151, Feb. 2015.

[12] H. Yang, Y. Zhang, J. Liang, J. Gao, P. D. Walker, and N. Zhang, "Sliding-mode observer based voltage-sensor-less model predictive power control of PWM rectifier under unbalanced grid conditions," *IEEE Trans. Ind. Electron.*, vol. 65, no. 7, pp. 5550–5560, Jul. 2018.

[13] F. Wang *et al.*, "Finite control set model predictive torque control of induction machine with a robust adaptive observer," *IEEE Trans. Ind. Electron.*, vol. 64, no. 4, pp. 2631–2641, Apr. 2017.

[14] T. Liu, T. Shi, and C. Xia, "Robust model predictive current control of grid-connected converter without alternating current voltage sensors," *IET Power Electron.*, vol. 7, no. 12, pp. 2934–2944, Dec. 2014.

[15] S. G. Jorge, J. A. Solsona, and C. A. Busada, "Control scheme for a single-phase grid-tied voltage source converter with reduced number of sensors," *IEEE Trans. Power Electron.*, vol. 29, no. 7, pp. 3758–3765, Jul. 2014.

[16] H. Bai, X. Wang, and F. Blaabjerg, "A grid-voltage-sensor-less resistive active power filter with series LC-filter," *IEEE Trans. Power Electron.*, vol. 33, no. 5, pp. 4429–4440, May 2018.

[17] R. Fantino, C. A. Busada, and J. A. Solsona, "Observer-based grid voltage sensor-less synchronization and control of a VSI-LCL tied to an unbalanced grid," *IEEE Trans. Ind. Electron.*, vol. 66, no. 7, pp. 4972–4981, Jul. 2019.

[18] S. Alireza Davari, D. Khaburi, F. Wang, and R. Kennel, "Using full order and reduced order observers for robust sensor-less predictive torque control of induction motors," *IEEE Trans. Power Electron.*, vol. 27, no. 7, pp. 3424–3433, Jul. 2012.

[19] F. Wang *et al.*, "An encoderless predictive torque control for an induction machine with a revised prediction model and EFOSMO," *IEEE Trans. Ind. Electron.*, vol. 61, no. 12, pp. 6635–6644, Dec. 2014.

[20] S. Vazquez, A. Marquez, J. I. Leon, L. G. Franquelo, and T. Geyer, "FCS-MPC and observer design for a VSI with output LC filter and sinusoidal output currents," in *Proc. 11th IEEE Int. Conf. Compat. Power Electron. Power Eng.*, 2017, pp. 677–682.

[21] H. T. Nguyen, E. Kim, I. Kim, H. H. Choi, and J. Jung, "Model predictive control with modulated optimal vector for a three-phase inverter with an LC filter," *IEEE Trans. Power Electron.*, vol. 33, no. 3, pp. 2690–2703, Mar. 2018.

[22] E. Kim, F. Mwasilu, H. H. Choi, and J. Jung, "An observer-based optimal voltage control scheme for three-phase UPS systems," *IEEE Trans. Ind. Electron.*, vol. 62, no. 4, pp. 2073–2081, Apr. 2015.

[23] P. Cortes, G. Ortiz, J. Yuz, J. Rodriguez, S. Vazquez, and L. Franquelo, "Model predictive control of an inverter with output LC filter for UPS applications," *IEEE Trans. Ind. Electron.*, vol. 56, no. 6, pp. 1875–1883, Jun. 2009.

[24] M. A. M. Cheema, J. E. Fletcher, M. Farshadnia, D. Xiao, and M. F. Rahman, "Combined speed and direct thrust force control of linear permanent-magnet synchronous motors with sensor-less speed estimation using a sliding-mode control with integral action," *IEEE Trans. Ind. Electron.*, vol. 64, no. 5, pp. 3489–3501, May 2017.